Modeling of quasi-supercontinuum laser linewidth and derivatives characteristics of InGaAs quantum dot broadband laser

C. L. Tan[a], Y. Wang[b], H. S. Djie[c], C. E. Dimas[a], Y. H. Ding[a], V. Hongpinyo[a], C. Chen[a], B. S. Ooi[a]
[a]Center for Optical Technologies and Department of Electrical and Computer Engineering, Lehigh University, 7 Asa Drive, Bethlehem, PA, USA 18015;
[b]OptiComp Corporation, Zephyr Cove, NV, USA 89448;
[c]JDS Uniphase Corporation, San Jose, CA, USA 95134;

ABSTRACT

We present the development of theoretical model based on multi-population rate equation to assess the broadband lasing emission in addition to the derivative optical gain and chirp characteristics from the supercontinuum InGaAs/GaAs self-assembled quantum-dot (QD) interband laser. The model incorporates the peculiar characteristics such as inhomogeneous broadening of the QD transition energies due to the size and composition fluctuation, homogeneous broadening due to the finite carrier lifetime in each confined energy states, and the presence of continuum states in wetting layer. We showed that the theoretical model agrees well with the experimental data of broadband QD laser. From the model, the broadband lasing characteristics can be ascribed to the large dispersion of QD with varying energy sub-bands and the change of de-phasing rate. These interesting characteristics can be attributed to the carrier localization in different dots that result in a system without a global Fermi function and thus an inhomogeneously broadened gain spectrum. Furthermore, our simulation results predict that the linewidth enhancement factor ($\alpha = 2$) from the ground state (GS) in this new class of semiconductor lasers is slightly larger but in the same order of magnitude as the values obtained in conventional QD lasers. The calculated gain spectrum shows similar magnitude order of material differential gain ($\sim 10^{-16}$ cm^2) and material differential refractive index ($\sim 10^{-20}$ cm^3) as compared to conventional QD lasers. The comparable derivative characteristics of broadband QD laser shows its competency in providing low frequency chirping as well as a platform for monolithic integration operation.

Keywords: Quantum-dot, semiconductor lasers, broadband laser diode, quasi-supercontinuum, linewidth enhancement factor, broad gain.

1. INTRODUCTION

Quantum-dot (QD) lasers have been investigated intensively in last two decades due to its expected superior performances over its quantum-well (QW) counterpart [1]. An important advantage of the QD laser diode is its ability to reach lasing threshold at very low current density (~11.7 A/cm^2) under continuous-wave (CW) room-temperature operation as compared to QW devices [2]. In addition, superior characteristics such as wide tunable range (~200 nm) at center wavelength of ~1.1 μm [3], high continuous-wave power emission of ~6.3 W at 980 nm [4], enhanced temperature stability of ~0.081 nm/K [5], etc, further proves the importance of QD nanostructures in the research field of semiconductor lasers. Nevertheless, the self-assembled QD nanostructures do not always meet the expected performance criteria due to the broadening optical gain as well as retarded carrier relaxation into the QD discrete energy states [6]. Although there have been a lot of studies being carried out on this broadening phenomenon [7-11], the mechanisms of the carrier dynamics processes in these nano-dimension QD crystal structures that contribute to broadband lasing spectra of QD devices is still understudied. The causes of these uncertainties of lasing bandwidth broadening are generally attributed to the carrier localization in noninteracting dot ensembles that is mainly due to the size fluctuations of QD [8] and homogeneous broadening that is due to the dephasing processes by both phonon scattering and Coulomb interaction with the injected carriers especially at room temperature [9-10].

Most recently, the observations of new multiple-state and broadband lasing action in semiconductor QD lasers have been attributed to the nature of inhomogeneous distribution of QD [12] together with incomplete clamping of excited state population at the ground state threshold [13]. One of the most exciting lasing properties is the quasi-supercontinuum lasing phenomenon that can find new applications in optical communications, low coherence biomedical

Physics and Simulation of Optoelectronic Devices XVII, edited by Marek Osinski, Bernd Witzigmann, Fritz Henneberger, Yasuhiko Arakawa, Proc. of SPIE Vol. 7211, 72110X · © 2009 SPIE · CCC code: 0277-786X/09/$18 · doi: 10.1117/12.808571

imaging, sensing, etc [14]. The experimental observation of the quasi-supercontinuum lasing is presented in Figure 1. This recent finding has led to the development of a theoretical investigation in accounting the supercontinuum broadband lasing signature [15]. Besides that, in order to further gain a comprehensive understanding of device physics and thus full exploration of all potential applications, a theoretical model is essential to assess not only the unique lasing behaviors of the quasi-supercontinuum QD laser but also its derivative optical characteristics such as optical differential gain, differential refractive index and most importantly, the magnitude of linewidth enhancement factor (α-parameter). These characteristics are important as they are directly related to the device performances such as lasing linewidth or signal dispersion, modulation-induced chirping, onset of coherence collapse induced by optical feedback and beam filamentation in gain-guided lasers [16-18].

In this paper, we report the lasing characteristics of broadband InGaAs/GaAs self-assembled quantum-dot (QD) interband lasers together with the calculated derivative characteristics obtained using the amplified spontaneous emission method. These interesting characteristics can be attributed to the inhomogeneously broadened gain spectrum and the change of dephasing rate. Furthermore, our simulation shows that the linewidth enhancement factor, material differential gain and material differential refractive index are in the same order of magnitude as compared to conventional QD lasers. The comparable derivative characteristics of broadband QD laser shows its competency in providing low frequency chirping as well as a platform for monolithic integration operation.

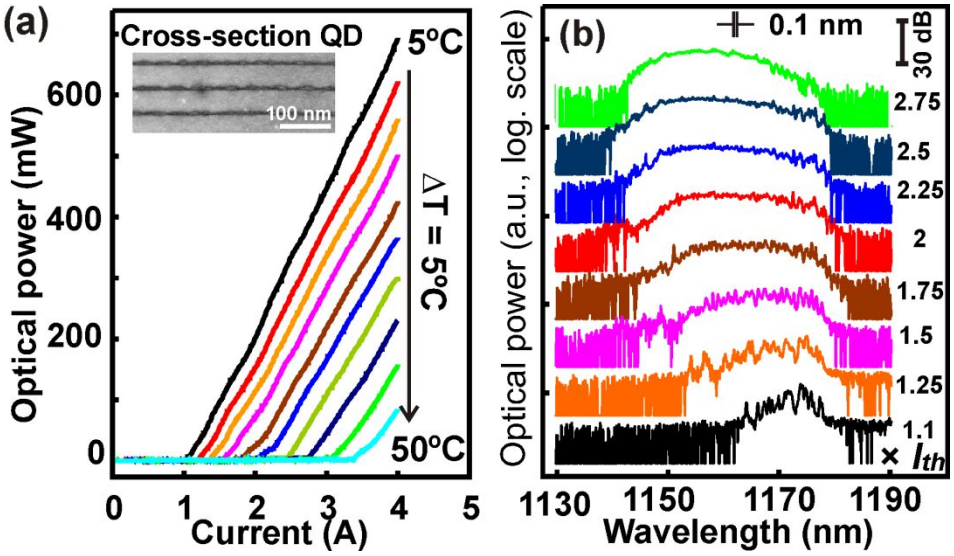

Fig. 1. [experimental data] (a) The L-I characteristics of InGaAs/GaAs QD laser with varying temperature operation. The inset shows the cross-section view of transmission electron microscope (TEM) image from QD active region. (b) The broadband laser spectra of QD laser (dimension of 50 × 800 μm^2) in a logarithmic scale under different current densities from 1.1 to 2.75 × I_{th} at 20ºC.

2. SIMULATION MODEL

2.1 Background

In our model, four discrete energy levels, i.e. wetting layer (WL), upper-continuum state (CS), ground state (GS) and excited state (ES) of each group of QD ensembles are incorporated in the multi-population rate equations. The calculation model is developed from the basic rate equations from each energy state of each group of QD ensembles, which are grouped by their respective resonant frequencies utilizing the QD laser theory [10]. The carrier thermal escape effect, inhomogeneous broadening of spatial distribution and homogeneous broadening of each single lasing mode are taken into account in the simulation model. Carrier thermal emission is assumed to occur among three energy levels in QD ensemble and also between CS and WL. The details of carrier population relaxation and reemission dynamics are schematically illustrated in Figure 2.

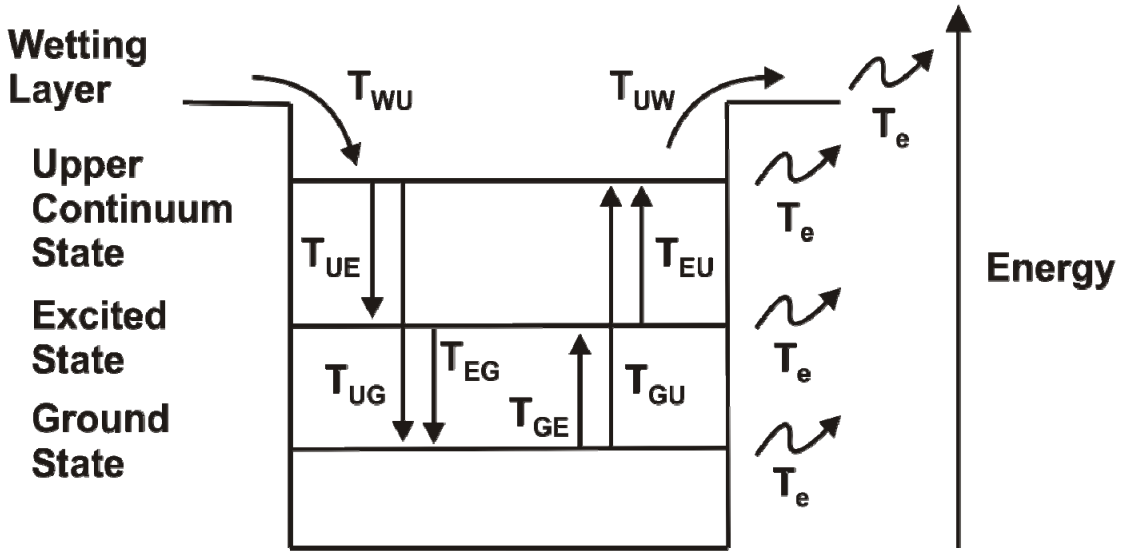

Fig. 2. Schematic of the energy band diagram that indicates the four different energy levels of wetting layer, upper continuum state, excited state and ground state of each group of QD ensemble with the inclusion of carrier capture and escape lifetime from the various states are shown.

As in most of the papers that treat rate-equation models for QD materials [17], we consider only the electron dynamics assuming the hole dynamics is so fast with respect to the electrons that all the gain and spontaneous emission dynamics properties of the QDs are almost determined by the electron dynamics in conduction band. The quantitative results [19] show that the dynamics is mainly limited by the electron relaxations and the effect of the different electron and hole distribution are significant only at very low bias of the QD laser diodes. This validates the justification of the model in view of the operation conditions considered in this paper. Besides that, a few similar assumptions are made in the simulation model [9]. Firstly, distribution of QDs is random in each layer of QD stacks. Secondly, there is no correlation among different dot layers and thus simplifying the calculation. Thirdly, all carriers in each group of QD ensembles have same relaxation and recombination rates. Lastly, carrier emission from higher dimensional confinement to lower confinement does not change with temperature but depends dominantly on the probability of carrier population. Besides that, a series of longitudinal cavity photon modes, $\underline{M}$, are taken into account over the interband transition energy of QDs to describe the interaction between the dots with different resonant energies and generated photons. For simplicity, our calculation model takes into account similar population of the grouping for QD ensembles as well as the number of photon modes, depending on the resonant energy of the interband transition. A wetting layer is considered as the reservoir of carriers to the three lower energy states in QDs [9, 17]. The QD laser structure used in the simulation includes mainly a 1 nm thick wetting layer that gives rise to one bound state of electron and holes together with QD of density $1.67\text{x}10^{23}$ m^{-3} and area of active region of $9.6\text{x}10^{-16}$ m^3. The overlap integral of electron and hole wavefunctions is assumed to be large [16] due to the columnar dots that are symmetric cylindrical structures, as compared to the dots that are pyramid-like structures. The 800 μm-long laser has as-cleaved facets that give a reflection coefficient $R = 0.3$.

2.2 Mathematical equations and simulation parameters

The rate equations in our model are as follows:

$$\frac{dN_w}{dt} = \frac{\eta_i I}{q} - \frac{N_w}{T_{wr}} - \frac{N_w}{\overline{T_{wu}}} - \frac{N_e}{T_e} + \frac{\sum N_{u,j}}{T_{uw}} \tag{1}$$

$$\frac{dN_{u,j}}{dt} = \frac{N_w G_n}{T_{wu,j}} + \frac{N_{g,j}}{T_{gu,j}} + \frac{N_{e,j}}{T_{eu,j}} - \frac{N_{u,j}}{T_{ug,j}} - \frac{N_{u,j}}{T_{ue,j}} - \frac{N_{u,j}}{T_{uw}} - \frac{N_{u,j}}{T_r} - \frac{N_{u,j}}{T_e} - \frac{c\Gamma}{n_r}\sum_m g_{mn} S_m \tag{2}$$

$$\frac{dN_{e,j}}{dt} = \frac{N_{u,j}}{T_{ue,j}} + \frac{N_{g,j}}{T_{ge,j}} - \frac{N_{e,j}}{T_{eu,j}} - \frac{N_{e,j}}{T_{eg,j}} - \frac{N_{e,j}}{T_r} - \frac{N_{e,j}}{T_e} - \frac{c\Gamma}{n_r}\sum_m g_{mn} S_m \tag{3}$$

$$\frac{dN_{g,j}}{dt} = \frac{N_{u,j}}{T_{ug,j}} + \frac{N_{e,j}}{T_{eg,j}} - \frac{N_{g,j}}{T_{gu,j}} - \frac{N_{g,j}}{T_{ge,j}} - \frac{N_{g,j}}{T_r} - \frac{N_{g,j}}{T_e} - \frac{c\Gamma}{n_r}\sum_m g_{mn} S_m \tag{4}$$

$$\Delta n_{gain}(E) = k\frac{\hbar c}{2E}\Gamma N_D \sum_l \sum_j D_l \frac{|P_l^{\sigma}|^2}{E_l}[(2P_{l,j}-1)G_n \frac{(E-E_{cv,l})/\pi}{(E-E_{cv,l})^2 + (\hbar\Gamma_{cv,l})^2}] \tag{5}$$

$$\Delta n_{plasma} = \Gamma_{SCH} K_n \frac{\Delta N_{SCH}}{E^2} + \Gamma_{WL} K_n \frac{\Delta N_{WL}}{E^2} \tag{6}$$

Equation (1) refers to the rate equation in WL. The symbol of N_w is the total carrier population of wetting layer, η_i is the internal quantum efficiency, I is the current injection, T_{wr} is the recombination lifetime constant in wetting layer, $\overline{T_{wu}}$ is the average carrier relaxation lifetime from WL to CS of each group of dot ensembles and T_{uw} is the excitation or emission lifetime from CS back to WL. The following three rate equations represent the carrier dynamics in CS, ES and GS, respectively. $N_{u,j}$, $N_{e,j}$ and $N_{g,j}$ is the carrier population of CS, ES and GS, respectively. T_r is the common recombination lifetime in each group of dot ensembles. In general, the subscripts of *w, u, e* and *g* refer to WL, CS, ES and GS, respectively. The subscript *j* refers to the *j*-th group of dot ensembles and the subscript *l* refers to u, e or g energy state. The linear optical gain g_{mn} that refers to the *n*-th group of dot ensemble contributing to the *m*-th mode photons is calculated based on the density-matrix equation, as suggested by Sugawara *et al* [9, 11]. The nonlinear optical gain is neglected. Γ is the optical confinement factor. The details of the developed model can be referred elsewhere [20].

The α-parameter of QD device can be obtained from the variation of the gain and refractive index produced by a small current step below threshold. Based on this platform, the α-parameter below threshold can be extracted from the model by studying the calculated amplified spontaneous emission (ASE) spectrum [17, 18]. The variation of the refractive index is given by the sum of the term linked through the Kramers-Kronig relation to the gain variation in QD and the term caused by the free carriers in WL [17, 18] as shown above. From the above equations, Δn_{gain} and Δn_{plasma} refer to the variation of refractive index due to gain variation and plasma effect, respectively. Γ_{SCH} and Γ_{WL} refer to the optical confinement factor of the separate confinement heterostructure (SCH) and WL, respectively. D_l refers to the degeneracy of each energy state *l*, and ΔN refers to the variation of the carrier in SCH and WL. For simplicity of extending the existing simulation model, only WL is taken into account to calculate the derivative characteristics of QD lasers. This model is then applied to QD lasers with different inhomogeneity levels in QD's size distribution in order to compare the α-parameter of the conventional and the broadband QD lasers. In principle, the α-parameter above threshold can also be calculated from the constructed rate equations [16, 21]. Melnik *et al.* [16] had developed a simple analytical formula that includes contributions from the energy transitions in the QDs and free carriers in the wetting layer. The equation is derived from the amplitude and frequency modulation responses using a simplified rate equation model and can be used, without loss of generality, to calculate the α-parameter of QD lasers [21], as follow.

$$\alpha = \alpha_{QD} + \alpha_{FC} \frac{\rho_{th} - 1 + \rho_{th} \dfrac{J}{J_{th}}}{2\rho_{th} - 1} \tag{7}$$

where ρ_{th} is the occupation probability of the QD ground state at threshold; J is the injection current; α_{QD} and α_{FC} are contributions to the α-parameter near threshold due to energy transitions in the QDs and free carrier plasma effects in the wetting layer, respectively.

3. RESULTS AND DISCUSSION

The calculation model is applied to InGaAs QD laser grown on GaAs substrate by different self-assembled growth modes in order to study in detail the effect of inhomogeneous broadening of QD ensembles on the optical gain and lasing spectra of QD laser. From [12], QDs grown by Stranski-Krastanov (SK) mode in molecular beam epitaxy (MBE) system (hereafter will refer to as conventional QD lasers) show smaller full width at half maximum (FWHM) of inhomogeneous broadening (hereafter will refer to as $\hbar\Gamma_{inh}$; 23 meV of bandwidth from photoluminescence measurement) as compared to dots that are grown by cycled monolayer deposition (CMD) mode in the same MBE system (hereafter will refer to as broadband QD lasers) that show 76 meV of bandwidth from photoluminescence characterization. The simulation model is applied initially to conventional QD lasers and the calculated results are shown in Figure 3 (conventional model), where the lasing spectra give similar results as reported by [11]. In these conventional QD lasers, the increase of injection will induce the changes of homogeneous broadening at different energy levels in a different way, as suggested or proposed by [12]. In broadband QD lasers, the simulation including proposed changes of homogeneous broadening with injection [15] give similar results as reported by [12]. The result is plotted in Figure 3 (proposed model). Figure 3 shows the FWHM of the lasing spectra obtained experimentally and theoretically, as a function of current injection in a highly inhomogeneous system. The continuous line and two types of dotted lines show the measured and calculated values of FWHM of the QD lasers, respectively. The increase of lasing bandwidth is basically observed in all the plotted data. In contrast, no significant increase of bandwidth but only the occurrence of two-states lasing from the conventional QD laser. Further increase of current at above two times threshold current results in a "saturation" of the lasing bandwidth. More carriers will fill up the higher energy levels in QDs when injection increases and thus the scattering lifetime of carriers decreases, which leads to the increase of $\hbar\Gamma_{h,e}$ followed by saturation of bandwidth [15]. At high injection current, we theoretically note that the linewidth is reduced due to the more dominant ES lasing. The dotted line calculated with conventional mechanism of carrier dynamics does not agree well with the measured results but the calculated results with new mechanism of carrier processes does [21]. From these results, the simulation of linewidth enhancement factor, material differential gain and material differential refractive index are evaluated.

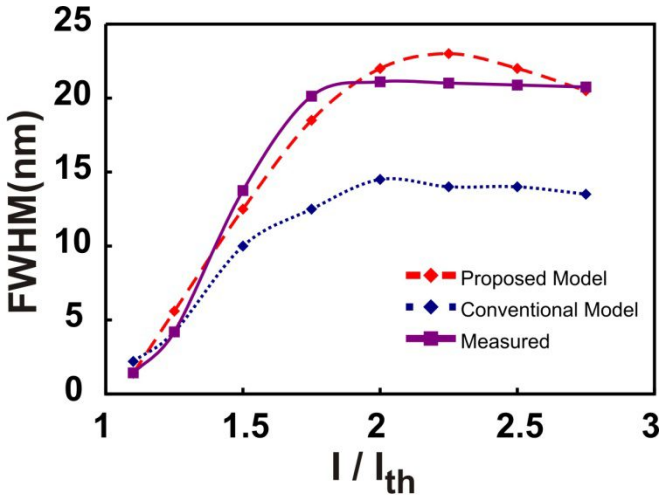

Fig. 3. The line-widths of lasing spectra under different levels of injections are shown for both measured (continuous line) and calculated data (dotted line). The calculated values include the data obtained from different mechanism of carrier processes in QDs.

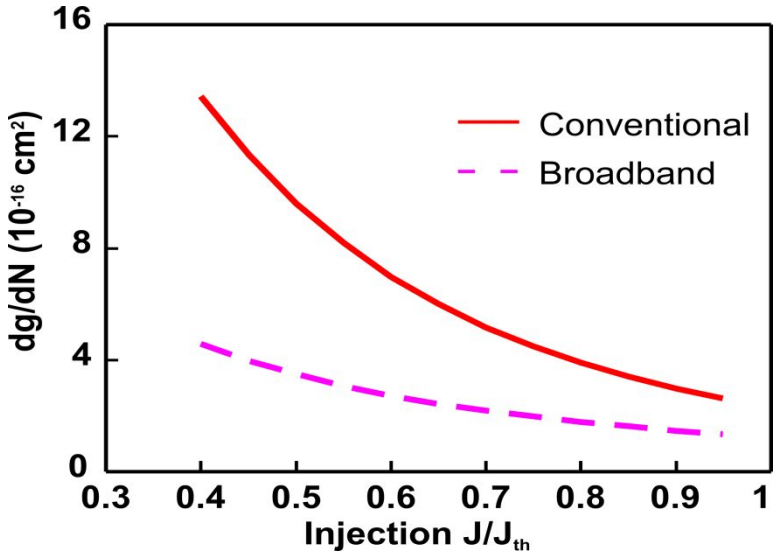

Fig. 4. The calculated differential gain (dg/dN) of both types of QD lasers, where conventional and broadband refers to QD lasers with conventional and proposed dephasing rate at each energy states, respectively.

The calculated differential gain with injection current for both types of QD lasers is shown in Figure 4, where broadband refers to broadband QD lasers with the proposed change of dephasing rate in each confined energy states [15]. The calculated values of differential gain near threshold are ~2.6 x 10^{-16} cm^2 and ~1.3 x 10^{-16} cm^2, for conventional and broadband QD lasers, respectively. The calculated differential gain of conventional QD lasers is similar to those obtained experimentally [22], validating the simulation model. However, the differential gain of the broadband laser is about two times lower than that of conventional systems leading to a much wider gain bandwidth. This effect is primarily the result of the extra large inhomogeneous broadening of QD systems [22]. It is worth noticing that the QD inhomogeneity here is not restricted to the fluctuation in the QD size or compositional, but to wider scopes that govern the fluctuations of quantized energy levels in QD system including the irregular arrangement of QD spatially and the variation of localized strain due to interdot interactions. Nevertheless, lower values of differential gain of the broadband lasers predict a smaller modulation bandwidth as compared to conventional system [21].

The calculated change in modal refractive index spectra in both conventional and broadband QD lasers shows that the latter gives a smaller variation of index change across the spectrum at all injections due to the larger carrier density that occupy the higher density states of energy levels that are well distributed among GS and ES [15]. As a result, the magnitude of differential refractive index of broadband QD lasers (~ -0.4 x 10^{-20} cm^3) is much smaller than that of conventional QD lasers (~ -0.7 x 10^{-20} cm^3) at near threshold, as presented in Figure 5. The similar calculated values of differential refractive index of conventional QD lasers with experimental data [22], again, verify the simulation model in predicting the α-parameter of these broadband QD lasers.

From the differential gain and refractive index, the α-parameters below threshold in both conventional and broadband QD lasers are calculated and as shown in Figure 6. At near threshold, the calculated α-parameter of broadband QD laser is ~ 3.3, which is slightly larger than that of conventional QD laser (α ~ 3). This may be attributed to the smaller magnitude decrease in differential refractive index as compared to the decrease of differential gain of broadband QD lasers with injection. Excessive carriers locating in the massive energy levels between ES and GS will tend to induce larger change of the refractive index with injection and thus leading to a larger magnitude of differential refractive index. In addition, from Kramers-Kronig relations, the asymmetry of the gain spectra will contribute to a larger differential refractive index as well, which in turn gives a larger value of α-parameter. From the calculated gain spectra, it is found that the gain spectra of the broadband QD lasers give a higher degree of asymmetrical as compared to the conventional systems. This may be due to the racing of lasing modes that occur among all possible transition energies in broadband systems. On the other hand, the range of transition energies that contributes to lasing in conventional QD lasers are much smaller [15]. Hence, conventional QD lasers will possess a more symmetrical gain spectrum at lasing modes. As a result, the broadband QD lasers will induce a larger differential refractive index around the lasing modes.

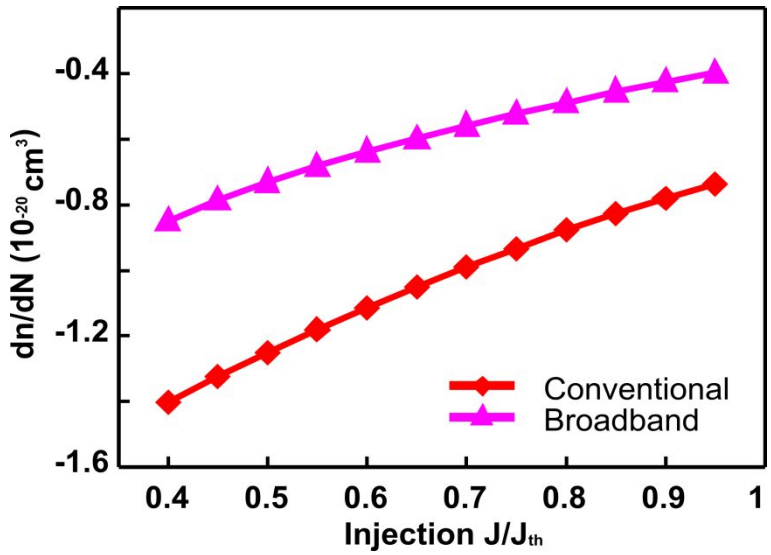

Fig. 5. The calculated differential refractive index of both types of QD lasers, where conventional and broadband refers to QD lasers with conventional and proposed dephasing rate at each energy states, respectively.

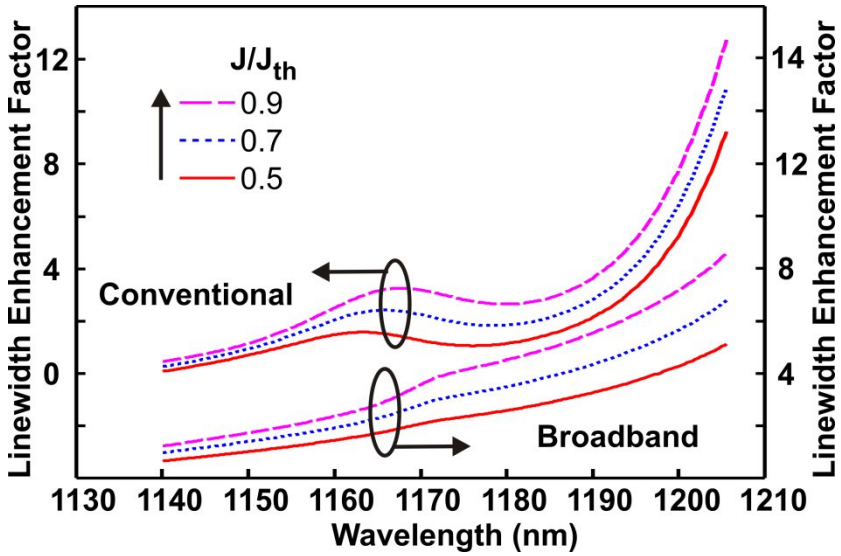

Fig. 6. . The calculated changes of linewidth enhancement factor with wavelength from both conventional and broadband QD lasers at different current injections.

Furthermore, the relaxation of carriers into a broader range of energy states will cause the retarded increment of the GS gain and thus a smaller differential gain is obtained in broadband QD lasers. As a result, both of the changes in differential gain and refractive index will increase the α-parameter of the broadband QD lasers as compared to the conventional systems at the GS transition energy. The change of α-parameter with different injections shows a good agreement with results reported from experimental measurements [23, 24]. In addition, the α-parameter above threshold increases rapidly with injection [16, 21]. The larger α-parameter of broadband QD lasers is resulted from the GS higher occupation probability at near threshold.

4. CONCLUSION

In conclusion, the experimental data of broadband laser signature agrees well with our theoretical calculation. From the model, broadband lasing effect can be explained by the large dispersion of QD size resulting in a broad lasing line from individual dot with varying energy sub-bands and the change of de-phasing rate in the active gain medium.

Besides that, the α-parameters of both conventional and broadband QD lasers below and above threshold injection are calculated and analyzed using the rate-equation model. The results give good indicator of the device characteristics such as filamentation in broad area devices and feedback sensitivity. The comparable values of α-parameter obtained in broadband QD lasers imply that broad gain QD medium is capable of providing low frequency chirping operation as well as an essential part of a monolithic QD integration platform.

ACKNOWLEDGEMENT

This work is supported by National Science Foundation (Grant No. 0725647), US Army Research Laboratory, Commonwealth of Pennsylvania, Department of Community and Economic Development. Authors are deeply grateful to Dr. Mitsuru Sugawara for very useful feedbacks on some parts of the theoretical model.

REFERENCES

[1] D. Bimberg, M. Grundmann, N. N. Ledentsov, M. H. Mao, Ch. Ribbat, R. Sellin, V. M. Ustinov, A. E. Zhukov, Zh. I. Alferov and J. A. Lott., "Novel infrared quantum dot lasers: theory and reality," Phys. Stat. Sol. (b) 224, 787-796 (2001).

[2] S. Freisem, G. Ozgur, K. Shavritranuruk, H. Chen and D. G. Deppe, "Very-low-threshold current density continuous-wave quantum-dot laser diode," Electon. Lett. 44, 670-671, (2008).

[3] P. M. Varangis, H. Li, G. T. Liu, T. C. Newell, A. Stintz, B. Fuchs, K. J. Malloy and L. F. Lester, "Low-threshold quantum dot lasers with 201 nm tuning range," Electron. Lett. 36, 1544-1545, (2000).

[4] B. Sumpf, S. Deubert, G. Erbert, J. Fricke, J. P. Reithmaier, A. Forchel, R. Staske and G. Trankle, "High-power 980 nm quantum dot broad area lasers," Electron. Lett. 39, 1655-1657, (2003).

[5] E-M Pavelescu, C. Gilfert, J. P. Reithmaier, A. Martin-Minguez and I. Esquivias, "GaInAs/(Al)GaAs quantum-dot lasers with high wavelength stability," Semicond. Sci. Technol. 23, 085022 1-4, (2008).

[6] M. Sugawara, Semiconductors and Semimetals, vol. 60, Academic, San Diego, (1999).

[7] L. V. Asryan and R. A. Suris, "Inhomogeneous line broadening and the threshold current density of a semiconductor quantum dot laser," Semicond. Sci. Technol. 11, 554-567, (1996).

[8] L. Harris, D. J. Mowbray, M. S. Skolnick, M. Hopkinson, and G. Hill, "Emission spectra and mode structure of InAs/GaAs self-organized quantum dot lasers," Appl. Phys. Lett. 73, 969-971, (1998).

[9] M. Sugawara, K. Mukai, Y. Nakata, H. Ishikawa, and A. Sakamoto, "Effect of homogeneous broadening of optical gain on lasing spectra in self-assembled InGaAs/GaAs quantum dot lasers," Phys. Rev. B 61, 7595-7603, (2000).

[10] P. Borri, W. Langbein, S. Schneider, U. Woggon, R. L. Sellin, D. Ouyang, and D. Bimberg, "Exciton relaxation and dephasing in quantum-dot amplifiers from room to cryogenic temperature," IEEE J. Sel. Top. Quantum Electron. 8, 984-991, (2002).

[11] M. Sugawara, N. Hatori, H. Ebe, M. Ishida, Y. Arakawa, T. Akiyama, K. Otsubo, and Y. Nakata, "Modeling room-temperature lasing spectra of 1.3-μm self-assembled InAs/GaAs quantum-dot lasers: Homogeneous broadening of optical gain under current injection," J. Appl. Phys. 97, 043523 1-8, (2005).

[12] H. S. Djie, B. S. Ooi, X. M. Fang, Y. Wu, J. M. Fastenau, W. K. Liu and M. Hopkinson, "Room-temperature broadband emission of an InGaAs/GaAs quantum dots laser," Opt. Lett. 32, 44-46, (2007).

[13] A. Markus, J. X. Chen, C. Paranthoen, A. Fiore, C. Platz and O. Gauthier-Lafaye "Simultaneous two-state lasing in quantum-dot lasers," Appl. Phys. Lett. 82, 1818-1820, (2003).

[14] B. S. Ooi, H. S. Djie, Y. Wang, C. L. Tan, J. C. M. Hwang, X. –M. Fang, J. M. Fastenau, A. W. K. Liu, G. T. Dang and W. H. Chang, "Quantum dashes on InP substrate for broadband emitter applications," IEEE J. Sel. Topic Quantum Electron. 14, 1230-1238, (2008).

[15] C. L. Tan, Y. Wang, H. S. Djie, and B. S. Ooi, "Role of optical broadening in the broadband semiconductor quantum-dot laser," Appl. Phys. Lett. 91, 061117 1-3, (2007).

[16] S. Melnik, G. Huyet, and A. V. Uskov, "The linewidth enhancement factor α of quantum dot semiconductor lasers," Opt. Express 14, 2950-2955, (2006).

[17] M. Gioannini,and I. Montrosset, "Numerical analysis of the frequency chirp in quantum-dot semiconductor lasers", IEEE J. Quantum Electron. 43, 941-949, (2007).

[18] M. Gioannini, A. Sevega, and I. Montrosset, "Simulations of differential gain and linewidth enhancement factor of quantum dot semiconductor lasers," Opt. Quantum Electron. 38, 381-394, (2006).
[19] A. Fiore and A. Markus, "Differential gain and gain compression in quantum dot lasers," IEEE J. Quantum Electron. 43, 287-294, (2007).
[20] C. L. Tan, Y. Wang, H. S. Djie, and B. S. Ooi, "The Role of optical gain broadening in the ultrabroadband InGaAs/GaAs interband quantum-dot laser," Comp. Mat. Sci. 44, 167-173, (2008).
[21] Z. Mi and P. Bhattacharya, "Analysis of the linewidth-enhancement factor of long-wavelength tunnel-injection quantum-dot lasers", IEEE J. Quantum Electron. 43, 363-369, (2007).
[22] A. A. Ukhanov, A. Stintz, P. G. Eliseev, and K. J. Malloy, "Comparison of the carrier induced refractive index, gain, and linewidth enhancement factor in quantum dot and quantum well lasers", *Appl. Phys. Lett.* vol. 84, pp. 1058-1060, (2004).
[23] J. Muszalski, J. Houlihan, G. Huyet, and B. Corbett, "Measurement of linewidth enhancement factor in self-assembled quantum dot semiconductor lasers emitting at 1310nm," *Electron. Lett.* vol. 40, no. 7, (2004).
[24] J. M. Vazquez, H. H. Nilsson, J. –Z. Zhang, and I. Galbraith, "Linewidth enhancement factor of quantum-dot optical amplifiers", *IEEE J. Quantum Electron.* vol. 42, pp. 986-993, (2006).